RJ 3886 (44174) 5/12/83
Mathematics

Research Report

A NUMERICAL STUDY OF CAPILLARY SPREADING OF A LIQUID LAYER

Jacob Fromm

IBM Research Laboratory
San Jose, California 95193

Research Division
Yorktown Heights, New York • San Jose, California • Zurich, Switzerland

RJ 3886 (44174) 5/12/83
Mathematics

A NUMERICAL STUDY OF CAPILLARY SPREADING OF A LIQUID LAYER

Jacob Fromm

IBM Research Laboratory
San Jose, California 95193

ABSTRACT: A numerical method for incompressible nonlinear flow is used to study the behavior of a fluid region that has an initial cylindrical lens configuration on a solid no-slip surface. Material contact angles that differ from the initial configuration, and the presence of a body force, produce motion that is calculated in cross section. Spreading rates are determined as a function of viscous to capillary forces.

I. INTRODUCTION

Macroscopic fluid behavior involving interfacial material surface energies is fraught with uncertainties. A static contact angle may be measured at equilibrium and defined as a constant interfacial property of a given liquid-solid surface. Dynamic behavior is another matter. Because of difficulties in measuring the contact angle to see if it always has the static value, its constancy in a moving system remains uncertain. Also, no-slip at the solid surface must harmonize with observed motion at a contact line. This further complicates matters. A common experimental view is that an apparent (time dependent) contact angle exists. A definition of this apparent contact may be stated as: the apparent contact angle is that angle value that may be extracted analytically on the basis of wetted area size with the surface retaining always a lens configuration. Clearly it must be time dependent, being initially 90° for a hemispherical cap, say. Unfortunately this provides no basis for a dynamic calculation since there is then no variation in curvature and hence no driving force for spreading to some other equilibrium configuration.

Constancy of the contact angle is sufficient for time dependent calculation with the proviso that the contact line is always fixed to its neighborhood of surface particles by a prescribed angle. Effectively this defines the velocity of the contact line at every instant of time. There appears to be no reason to assume any time variation of the contact angle itself. The separate issue of no-slip cannot be addressed in detail in a continuum description. We here sidestep the question of discontinuity of velocity derivatives along the solid surface, accepting the notion that a continuous transition zone exists. This is common in fluid dynamic descriptions where incorporated mathematical discontinuities are in conflict with reality. Since the numerical method deals in discrete quantities, much larger to be sure than a sharp transition zone, it nevertheless avoids an impasse. A transition zone takes on a scale

of the grid distance which is the limit of definition of the numerical approximation. Local errors can of course be large and of concern. However, with an otherwise intractable problem, it seems that numerical integration is the only recourse, providing a broad view of acceptable accuracy and a utilitarian need. This, at the sacrifice of detailed information in transition zones but the capacity to illuminate a range of flow dynamics that do not necessarily depend upon small scale.

Background discussion of the status of knowledge of spreading of liquids can be found in the review article by Dussan[1] which includes a long list of references. Perhaps numerical solutions can have value in basic work by providing a point of departure for molecular scale studies. We here take the view that a missing aspect of the overall problem is a theoretical bench mark for diverse experiments which are currently too spotty to be comprehensive. Sparseness of experimental data is not surprising, considering the difficulty of making good measurements and the problem of assimilating data on a broad spectrum of materials.

Currently, numerical work on spreading of liquids is limited to two dimensional studies. Since we are interested in a possible body force in the plane of a no-slip surface and also in possible differing liquid-solid interface energies within the range of a layer, we have chosen a rectangular geometry for calculation. For spread rate studies we consider an initial configuration as given in Figure 1. All, constant area, equilibrium configurations are definable, in rectangular geometry, in terms of a static contact angle γ as

$$r_0^2 = \frac{\pi}{2\gamma - \sin 2\gamma} \tag{1}$$

where r_0 is the radius of the enclosing arc. The height of the cylindrical lens of fluid above the solid surface is given by

$$h = r_0(1 - \cos \gamma) \tag{2}$$

and the half length along the solid surface by

$$\ell = r_0 \sin \gamma \, . \tag{3}$$

The $\gamma_1=\gamma_2=90°$ configuration with area $A=\pi/2$ provides the basis for scaling the calculations with a characteristic length r as indicated in Figure 1. The "capillary wave velocity[2]" provides a velocity scale v with σ the surface tension coefficient and ρ the fluid density. A time scale t follows from these definitions.

In the text we will briefly consider the differential form of the calculation method without details of the numerical algorithms (the numerical procedures are given in reference 3). This is followed by a discussion of solutions chosen to illustrate typical timewise behavior. Nonlinear examples are chosen because of their interesting oscillatory behavior both with contact angles less than and greater than 90°. An example with an in plane body force is included. Reference 3 contains an example of spreading in the linear range of the parameters and a case of differing contact energies.

A summary of spread rates based upon first arrival time at a distance ℓ (Eq. (3)) for $\gamma_1=\gamma_2=45°$ is considered as a function of the ratio of viscous to capillary forces. The simplicity of the relationship allows an approximate analytic expression to be given and it is assumed that future work will permit a similar characterization at other contact angles.

II. THE GOVERNING EQUATIONS

The numerical method is one that uses explicit time differences on a fixed rectangular grid system but includes local moving coordinate systems tied to discrete positions of the free surface (see Figure 1). A so-called "vorticity-streamfunction" method for interior flow is augmented with a velocity potential and a secondary streamfunction to provide the necessary free surface boundary conditions.

We first scale the problem with

$$W/R = \left(\frac{\rho v^2}{\sigma r} \right)^{1/2} \qquad \text{and} \qquad B = \frac{\rho r^2 a}{\sigma} , \tag{4}$$

where W/R is a ratio of Weber number to Reynolds number and B is the Bond number. The latter contains an acceleration "a" which for our immediate interest is directed parallel to the solid surface. The Bond number is a ratio of body to capillary forces.

Interior flow equations may be written in terms of vorticity (ω) and streamfunction (Q) as

$$\frac{\partial \omega}{\partial t} + \frac{\partial u\omega}{\partial x} + \frac{\partial v\omega}{\partial y} = \frac{W}{R} \left(\frac{\partial^2 \omega}{\partial x^2} + \frac{\partial^2 \omega}{\partial y^2} \right) \tag{5}$$

and

$$\frac{\partial^2 Q}{\partial x^2} + \frac{\partial^2 Q}{\partial y^2} = - \omega , \tag{6}$$

where

$$u = \frac{\partial Q}{\partial y} \qquad \text{and} \qquad v = - \frac{\partial Q}{\partial x} \tag{7}$$

are velocities in the x and y directions, respectively.

If we consider the velocities to be composed of irrotational and solenoidal parts (Ref. 4), we may write

$$u = u_i + u_s = \frac{\partial \phi}{\partial x} + \frac{\partial \psi}{\partial y} ,$$
$$v = v_i + v_s = \frac{\partial \phi}{\partial y} - \frac{\partial \psi}{\partial x} , \tag{8}$$

where ϕ is a velocity potential and ψ a secondary streamfunction. Since we do not have potential flow, except perhaps at the very first instant of a timewise calculation, neither Q nor ψ are harmonic with ϕ. But, since we have incompressible flow, ϕ nevertheless satisfies

$$\frac{\partial^2 \phi}{\partial x^2} + \frac{\partial^2 \phi}{\partial y^2} = 0 \tag{9}$$

in the fluid interior while ψ, the secondary streamfunction, satisfies (6) with boundary conditions different than those on Q.

At the free surface we are interested in expressing u and v in terms of normal (u_η) and tangential (u_τ) components in (τ,η) reference frames. Thus (u,v) are related to (u_τ,u_η) by a rotational transformation so that

$$u_\tau = u \cos \alpha + v \sin \alpha$$
$$u_\eta = -u \sin \alpha + v \cos \alpha \tag{10}$$

where α is an angle, varying along the surface, relating τ to x, say.

We may develop the flow equations at the free surface, by transformation to the local systems. Continuity becomes

$$\frac{\partial u_\tau}{\partial \tau} + \frac{\partial u_\eta}{\partial \eta} + u_\tau \frac{\partial \alpha}{\partial \eta} - u_\eta \frac{\partial \alpha}{\partial \tau} = 0 . \tag{11}$$

Surface stress conditions (see for example Ref. 5) are transformed into surface coordinate form as

$$\text{Normal Stress: } \left(\frac{P}{\rho}\right) - \left(\frac{P}{\rho}\right)_g = -\frac{\partial\alpha}{\partial\tau} + 2\,\frac{W}{R}\left(\frac{\partial u_\eta}{\partial\eta} + u_\tau\,\frac{\partial\alpha}{\partial\eta}\right) \tag{12}$$

$$\text{Tangential Stress: } \frac{\partial u_\eta}{\partial\tau} + u_\tau\,\frac{\partial\alpha}{\partial\tau} + \frac{\partial u_\tau}{\partial\eta} - u_\eta\,\frac{\partial\alpha}{\partial\eta} = 0 \tag{13}$$

where P is the pressure, defined in locally adjacent positions in the liquid and gas. The unit coefficient on the curvature $\left(\frac{\partial\alpha}{\partial\tau}\right)$ has to do with our method of scaling. Finally we will be interested in the surface vorticity which upon transformation is

$$\omega = \frac{\partial u_\eta}{\partial\tau} + u_\tau\,\frac{\partial\alpha}{\partial\tau} - \frac{\partial u_\tau}{\partial\eta} + u_\eta\,\frac{\partial\alpha}{\partial\tau}\,. \tag{14}$$

Beginning with "Lamb's" form of the momentum equations, we are led to surface equations

$$\frac{\partial u_\tau}{\partial t} + \frac{1}{2}\,\frac{\partial}{\partial\tau}\left(u_\tau^2 + u_\eta^2\right) - u_\eta\omega = -\frac{\partial\left(\frac{P}{\rho}\right)}{\partial\tau} - \frac{W}{R}\,\frac{\partial\omega}{\partial\eta} + B_\tau\,, \tag{15}$$

$$\frac{\partial u_\eta}{\partial t} + \frac{1}{2}\,\frac{\partial}{\partial\eta}\left(u_\tau^2 + u_\eta^2\right) + u_\tau\omega = -\frac{\partial\left(\frac{P}{\rho}\right)}{\partial\eta} + \frac{W}{R}\,\frac{\partial\omega}{\partial\tau} + B_\eta\,. \tag{16}$$

We may use (11) to remove normal derivatives from (12) and use (13) to remove normal derivatives from (14) so that final expressions for P and ω as required in (15) and (16) are

$$\frac{P}{\rho} = -\frac{\partial\alpha}{\partial\tau} + 2\,\frac{W}{R}\left(u_\eta\,\frac{\partial\alpha}{\partial\tau} - \frac{\partial u_\tau}{\partial\tau}\right)\,, \tag{17}$$

and

$$\omega = 2\left(u_\tau \frac{\partial \alpha}{\partial \tau} + \frac{\partial u_\eta}{\partial \tau} \right) , \tag{18}$$

where $(P/\rho)_g$ has here arbitrarily been taken to be zero.

As with (8) we can express the surface velocities in terms of irrotational and solenoidal parts

$$\begin{aligned} u_\tau &= u_\tau^i + u_\tau^s = \frac{\partial \phi}{\partial \tau} + \frac{\partial \psi}{\partial \eta} = \frac{\partial Q}{\partial \eta} \\ u_\eta &= u_\eta^i + u_\eta^s = \frac{\partial \phi}{\partial \eta} - \frac{\partial \psi}{\partial \tau} = - \frac{\partial Q}{\partial \tau} \end{aligned} \tag{19}$$

Using (19) we can split the momentum Eqs. (15) and (16) and write for $\dot{\phi} = \frac{\partial \phi}{\partial t}$ and $\dot{\psi} = \frac{\partial \dot{\psi}}{\partial t}$

$$\frac{\partial \dot{\phi}}{\partial \tau} = - \frac{\partial \left(\frac{P}{\rho} \right)}{\partial \tau} + B_x \frac{\partial x}{\partial \tau} + B_y \frac{\partial y}{\partial \tau} - \frac{1}{2} \frac{\partial}{\partial \tau} \left(u_\tau^2 + u_\eta^2 \right) \tag{20}$$

$$\frac{\partial \dot{\psi}}{\partial \tau} = - \frac{W}{R} \frac{\partial \omega}{\partial \tau} + u_\tau \omega \tag{21}$$

$$\frac{\partial \dot{\phi}}{\partial \eta} = - \frac{\partial \left(\frac{P}{\rho} \right)}{\partial \eta} + B_x \frac{\partial x}{\partial \eta} + B_y \frac{\partial y}{\partial \eta} - \frac{1}{2} \frac{\partial}{\partial \eta} \left(u_\tau^2 + u_\eta^2 \right) \tag{22}$$

$$\frac{\partial \dot{\psi}}{\partial \eta} = - \frac{W}{R} \frac{\partial \omega}{\partial \eta} + u_\eta \omega \, . \tag{23}$$

We do not need (22) and (23), they are included only for completeness. The seemingly inconsistent $(u_\tau \omega)$ term in (21) compared to $(u_\eta \omega)$ in (23) reflects a property of the streamfunction.

The calculation procedure is to obtain $(\dot{\phi},\dot{\psi})$ with (20) and (21) and hence (ϕ,ψ) at the surface. Now u^s_η follows directly from ψ but u^i_η requires solution of (9) in the fluid interior. Assuming this to be done, Q at the surface follows from the second of (19). We next solve (6) in the interior and extract u_η at the surface.

The inverse of (10) gives u and v at the surface, except at the no-slip boundary where u and v are given, that is, v=0 and u follows from updated contact positions satisfying a "static" contact angle condition. The surface configuration is next modified in the Lagrangian sense, *i.e.*,

$$\frac{dx}{dt} = u\ , \qquad \frac{dy}{dt} = v\ . \tag{24}$$

This leads to revised angles α of the local frames relative to the global (x,y) reference frame. Through small discrete time steps of the vorticity Eq. (5) and the time dependent free surface Eqs. (20) and (21), we repeatedly solve the ϕ and Q elliptic equations in a forward march of the solutions toward equilibrium.

III. NUMERICAL RESULTS

The configuration as illustrated in Figure 1 serves as the initial solution for spreading calculations. It is an idealization, perhaps difficult to establish experimentally, but appropriate here. Motion from this constant curvature shape is initiated by setting the free surface particles which are in contact with the no-slip surface to a new position. Relative to its nearest neighbor, each new contact particle position defines an input contact angle with the horizontal. The modified curvature, while very localized, is instantly "felt" throughout the liquid in the incompressible case with pressure gradients such that flow converges upon the contact lines.

Figures 2a, 2b and 2c ($W/R=0.05$, $\gamma_1=\gamma_2=45°$) illustrate in cross section a selected set of times after the onset of motion. The cylindrical lens of fluid is centered at 3.5 units in the horizontal. Streamlines are the solid lines with negative contours containing tick marks. The central streamline is the "zero" dividing streamline that intersects the solid surface. The *apparently* normal (to the streamlines) contours are lines of constant velocity potential. They do not have the special relationship to streamlines that exists in potential flow, also they do not represent the full solution and are included here to illustrate the role ϕ plays in calculation. We have chosen the potential to be "forever" zero at the crest of the initial configuration. At the first time illustrated in Figure 2 the velocity potential takes on its most positive values at the contact lines and somewhat negative values where the surface has the highest downward (convex) curvature. Details of the contours at each time of the sequence are given in Table I.

Clearly the configuration does not retain the shape of a circular arc. In the linear range ($W/R>0.5$) (see later discussion) one does not have the early time "pyramid" shape of the surface, tending throughout to have a more lens shaped surface except for the meniscus. For $\gamma_1=\gamma_2=45°$, equilibrium has $r_0=2.34$ for the final configuration with height above the surface $h=0.68$ units and half length along the solid surface $\ell=1.65$ units. At the final time of Figure 2a this configuration is nearly realized. Because of inertia and an apparent broad minimum in the surface energy, later time solutions overshoot equilibrium. The time variation of h and ℓ are illustrated in Figure 3. Between times $t=1.84$ and $t=2.25$ retraction from overshoot begins (note that at $t=2.25$ the ticked streamlines appear on the right rather than on the left as earlier). The streamlines have a sharp bend with flow tending to parallel the solid surface because the reversed boundary layer has yet to be established.

In Figure 2c the retracting flow again passes equilibrium with transition to outward flow. The transition time is nearly captured at time t=4.37. Here again there is essentially no boundary layer. In Table I the transitions are fairly well defined by the interchange of extremals in the velocity potential.

Finally in Figure 4 we give a spread time curve for $\gamma_1=\gamma_2=45°$ for a logrithmic range of values of W/R. The times are based upon first arrival to $\ell=1.65$ units (the equilibrium half distance for $\gamma=45°$). Spread times at other contact angles have not as yet been calculated. A surprising aspect of Figure 4 is that the spread time (as defined) is nearly a constant function of W/R in the nonlinear range with a value of t (nondimensional) ~1.25. The linear range (W/R>0.5) spread time can be expressed as

$$t = 1.25 + 3\,\frac{W}{R}\,. \tag{26}$$

We have indicated a dotted line in the range where nonlinear effects first become apparent. The reason for this is that we observed a cusp of more rapid spreading that could have been either physical or numerical. Since it could not be adequately explained we tentatively leave the question open. There is the possibility of anomalous interaction of the boundary layer and the meniscus in this range. Outside this sharp division, calculations were made without difficulty.

In Figures 5a and 5b we consider a contrary situation to Figure 2 with γ greater than 90°. Again with W/R=0.05 but with $\gamma_1=\gamma_2=110°$, contraction first occurs. Transition from contraction to spreading occurs near t=1.28 of Figure 5a and from spreading to a second contraction near t=3.16 of Figure 5b. The detailed time data of Figures 4a and 4b are given in Table II.

In Figure 6 we begin with an equilibrium configuration of $\gamma_1=\gamma_2=45°$ but impose an in-plane body force (B=−0.2) directed to the left. Even though the static contact angle exists throughout, a flattening of the surface takes place. Rather than a leading and trailing contact angle we have a constant contact angle but differing leading and trailing velocities. The tear drop shape so familiar in three dimensional flow under gravity is much less apparent in a liquid layer (two dimensional). The details of the plots of Figure 6 are given in Table III. We have not carried this calculation out far enough to see if an ultimate steady configuration emerges; differing accelerations of the contact lines are still taking place at the last time illustrated.

TABLE I

t	ΔQ	Q_{min}	Q_{max}	$\Delta\phi$	ϕ_{min}	ϕ_{max}
0.250	1/32	-2.46×10^{-1}	2.46×10^{-1}	1/32	-9.03×10^{-2}	3.27×10^{-1}
0.375	1/32	-2.43×10^{-1}	2.51×10^{-1}	1/32	-2.27×10^{-2}	4.21×10^{-1}
0.500	1/32	-2.36×10^{-1}	2.39×10^{-1}	1/16	0.0	5.03×10^{-1}
0.687	1/32	-2.38×10^{-1}	2.50×10^{-1}	1/16	0.0	5.36×10^{-1}
0.906	1/32	-2.16×10^{-1}	2.03×10^{-1}	1/32	0.0	4.55×10^{-1}
1.34	1/64	-1.06×10^{-1}	1.04×10^{-1}	1/64	~0.0	1.77×10^{-1}
1.57	1/128	-5.97×10^{-2}	5.65×10^{-2}	1/256	~0.0	4.26×10^{-2}
1.84	1/256	-1.88×10^{-2}	1.81×10^{-2}	1/128	-8.52×10^{-2}	~0.0
2.25	1/256	-2.36×10^{-2}	1.87×10^{-2}	1/64	-2.01×10^{-1}	0.0
2.53	1/128	-5.74×10^{-2}	5.77×10^{-2}	1/32	-2.99×10^{-1}	0.0
2.78	1/64	-9.03×10^{-2}	9.56×10^{-2}	1/32	-3.80×10^{-1}	0.0
3.24	1/64	-1.15×10^{-1}	1.24×10^{-1}	1/32	-4.46×10^{-1}	0.0
3.49	1/64	-1.11×10^{-1}	1.00×10^{-1}	1/32	-3.31×10^{-1}	0.0
4.37	1/1024	-9.43×10^{-3}	9.34×10^{-3}	1/1024	0.0	1.61×10^{-2}
5.14	1/64	-8.93×10^{-2}	8.54×10^{-2}	1/32	0.0	2.57×10^{-1}

TABLE II

t	ΔQ	Q_{min}	Q_{max}	$\Delta\phi$	ϕ_{min}	ϕ_{max}
0.0031	1/64	-1.02×10^{-1}	1.01×10^{-1}	1/64	-1.47×10^{-1}	4.44×10^{-3}
0.250	1/32	-1.51×10^{-1}	1.52×10^{-1}	1/64	-1.78×10^{-1}	1.88×10^{-2}
0.569	1/32	-1.42×10^{-1}	1.39×10^{-1}	1/64	-2.36×10^{-1}	0.0
0.883	1/64	-8.79×10^{-2}	8.78×10^{-2}	1/64	-1.38×10^{-1}	~0.0
1.28	1/512	-1.22×10^{-2}	1.29×10^{-2}	1/1024	0.0	1.31×10^{-2}
1.86	1/128	-5.55×10^{-2}	5.60×10^{-2}	1/64	~0.0	1.27×10^{-1}
2.25	1/64	-7.88×10^{-2}	7.98×10^{-2}	1/64	0.0	1.76×10^{-1}
2.63	1/128	-6.15×10^{-2}	6.11×10^{-2}	1/64	0.0	1.36×10^{-1}
3.16	1/512	-8.26×10^{-3}	8.25×10^{-3}	1/256	~0.0	3.49×10^{-2}
3.66	1/128	-4.32×10^{-2}	4.31×10^{-2}	1/128	-6.73×10^{-2}	0.0

TABLE III

t	ΔQ	Q_{min}	Q_{max}	$\Delta\phi$	ϕ_{min}	ϕ_{max}
0.484	1/128	-4.92×10^{-2}	0.0	1/64	-1.09×10^{-1}	1.05×10^{-1}
1.99	1/32	-2.19×10^{-1}	0.0	1/16	-4.71×10^{-1}	4.51×10^{-1}
3.62	1/16	-3.90×10^{-1}	0.0	1/8	-8.04×10^{-1}	7.23×10^{-1}
5.24	1/16	-4.35×10^{-1}	0.0	1/8	-1.06	7.75×10^{-1}
6.16	1/16	-4.60×10^{-1}	0.0	1/4	-1.24	8.04×10^{-1}

REFERENCES

1. E. B. Dussan V, "On the Spreading of Liquids on Solid Surfaces: Static and Dynamic Contact Lines," *Ann. Rev. Fluid Mech.* 11, 371-400 (1979).

2. J. W. S. Rayleigh, *The Theory of Sound*, Vol. 2 (Dover, 1945), p. 351.

3. J. E. Fromm, "Free Surface Calculation with Application to Drop and Layer Spreading," *IBM Research Report RJ3871.*

4. H. Lass, *Vector and Tensor Analysis* (McGraw-Hill Book Company, Inc., New York, 1950).

5. G. K. Batchlor, *An Introduction to Fluid Dynamics* (Cambridge University Press, Cambridge, 1967).

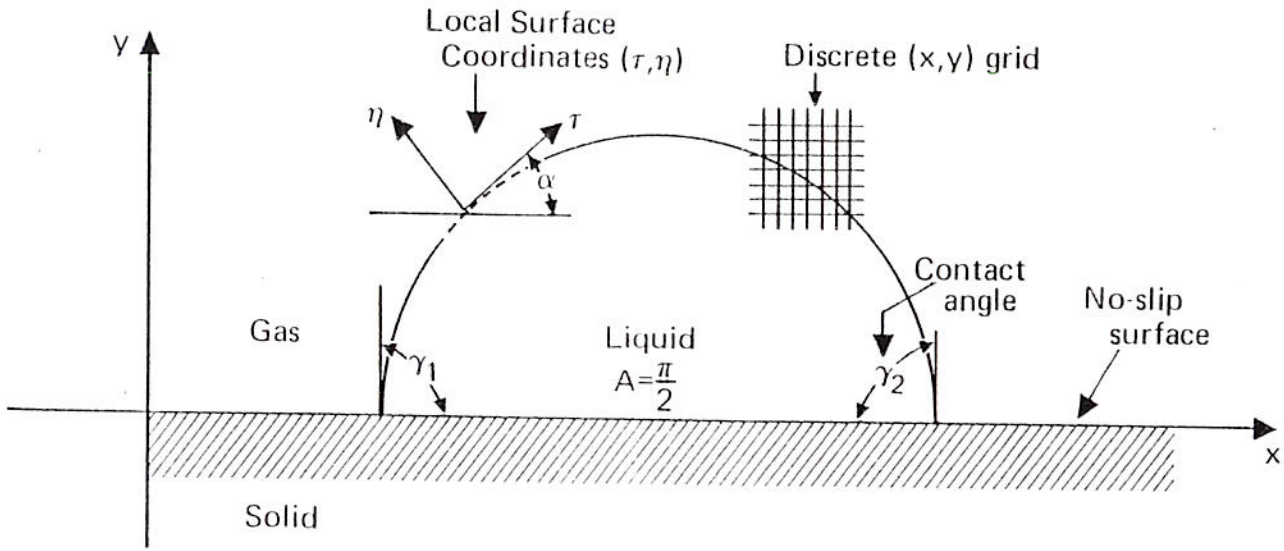

$$\text{Characteristic length} \quad r = \left(\frac{2A}{\pi}\right)^{1/2}$$

$$\text{velocity} \quad v = \left(\frac{\sigma}{\rho r}\right)^{1/2}$$

$$\text{time} \quad t = \left(\frac{\rho r^3}{\sigma}\right)^{1/2}$$

Figure 1. Problem geometry and scale.

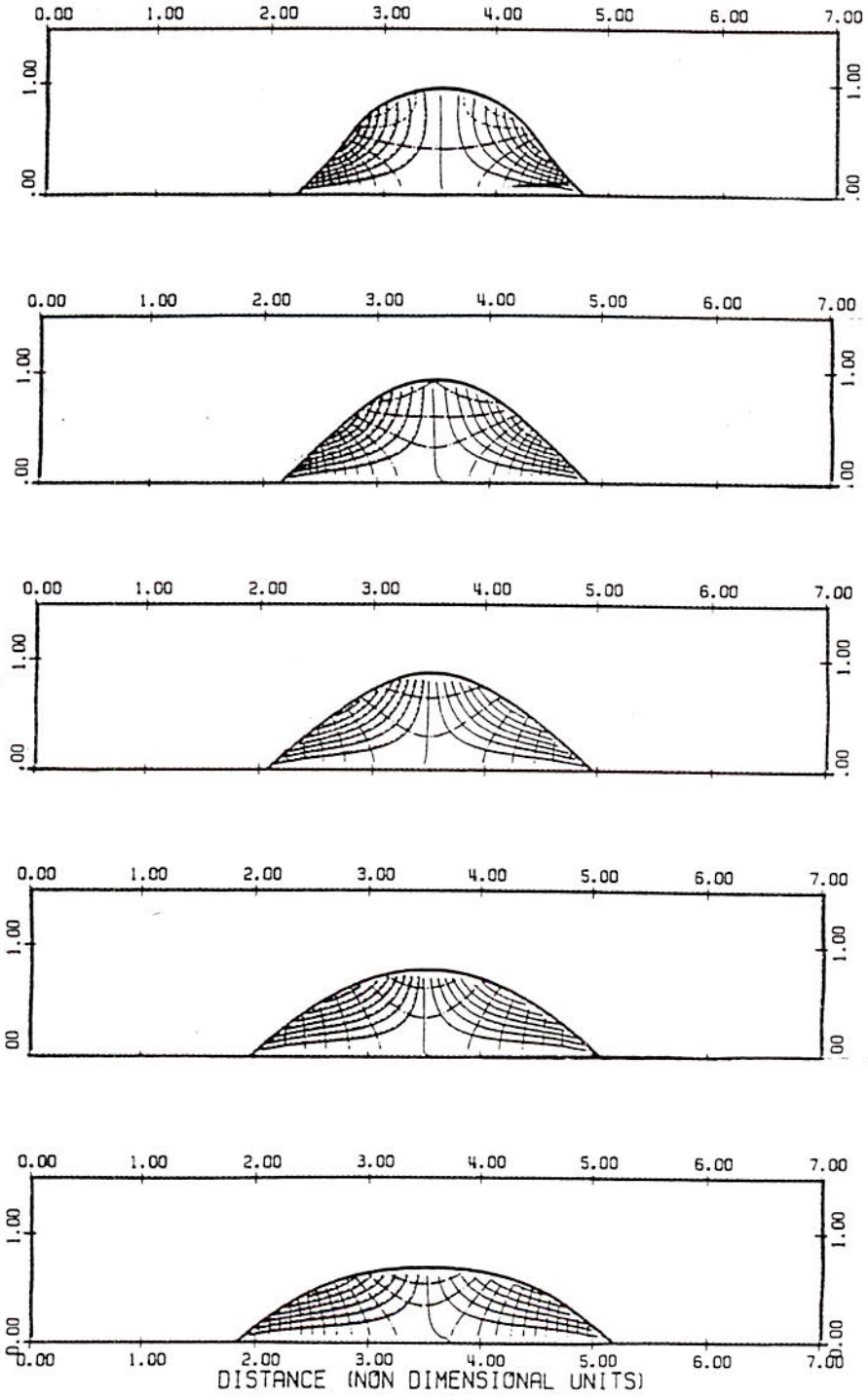

Figure 2a. Time sequence of solutions for $W/R=0.05$, $\gamma_1=\gamma_2=45°$ and $B=0$. See Table I.

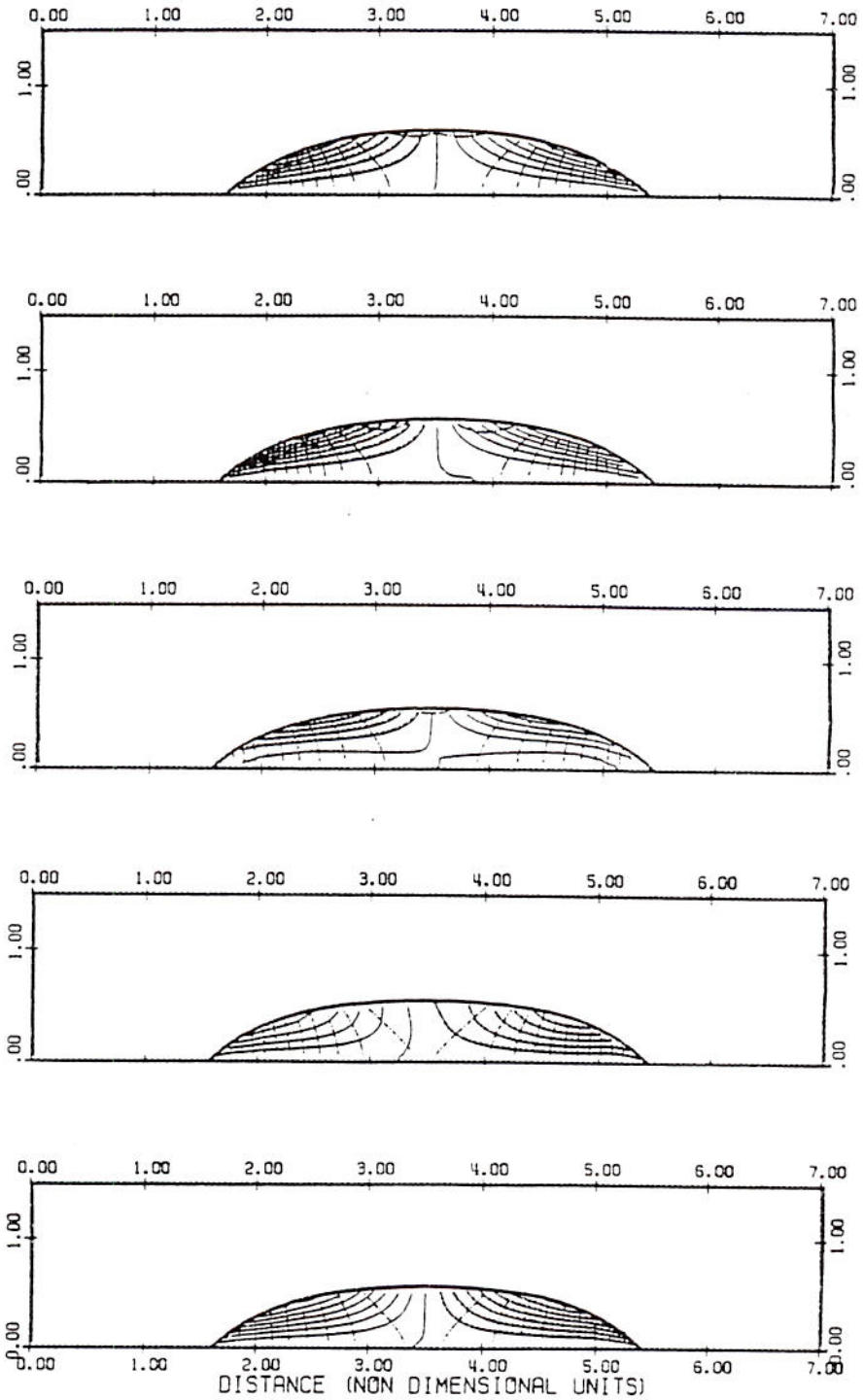

Figure 2b. Continuation of Figure 2a. See Table I.

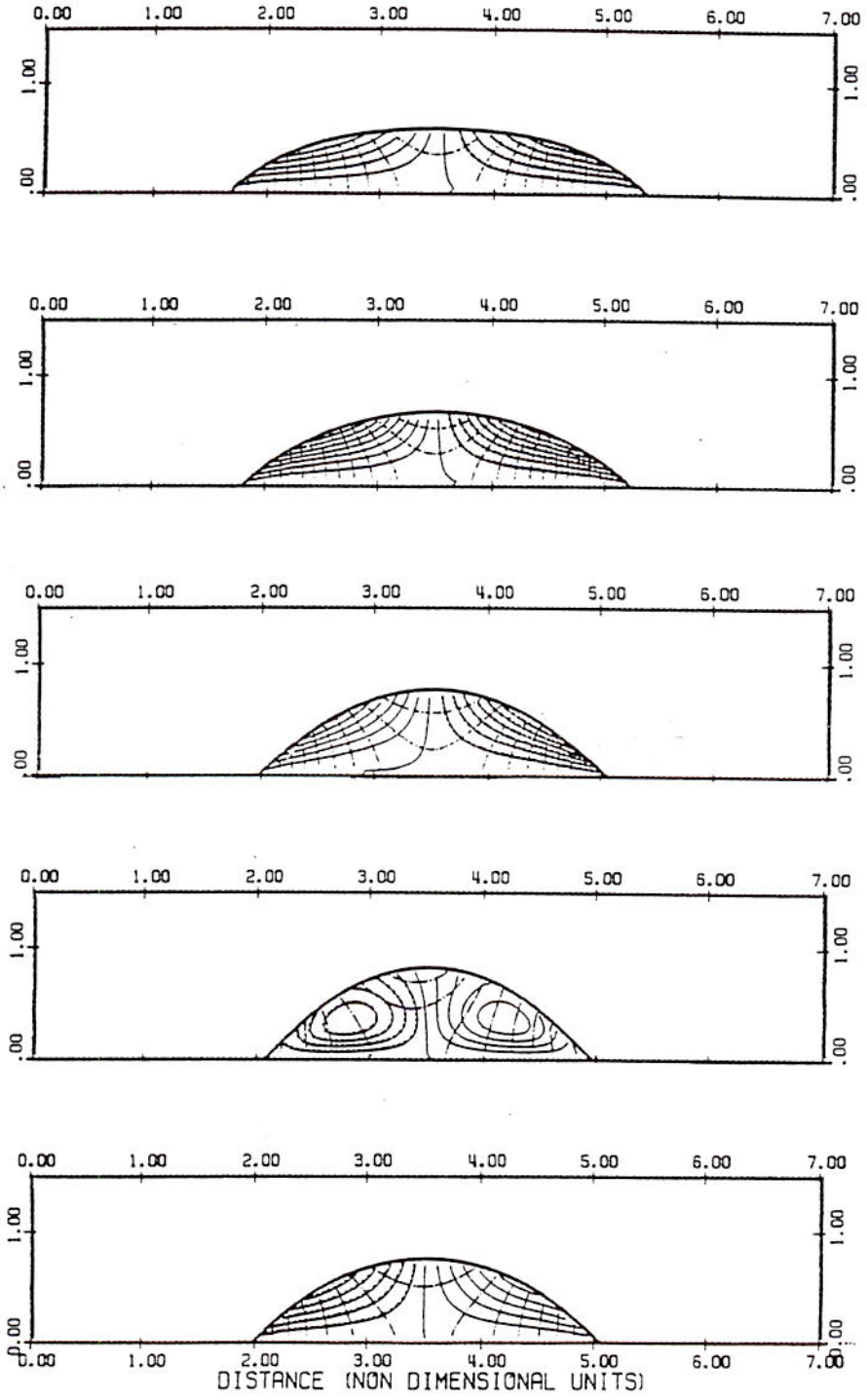

Figure 2c. Continuation of Figure 2b. See Table I.

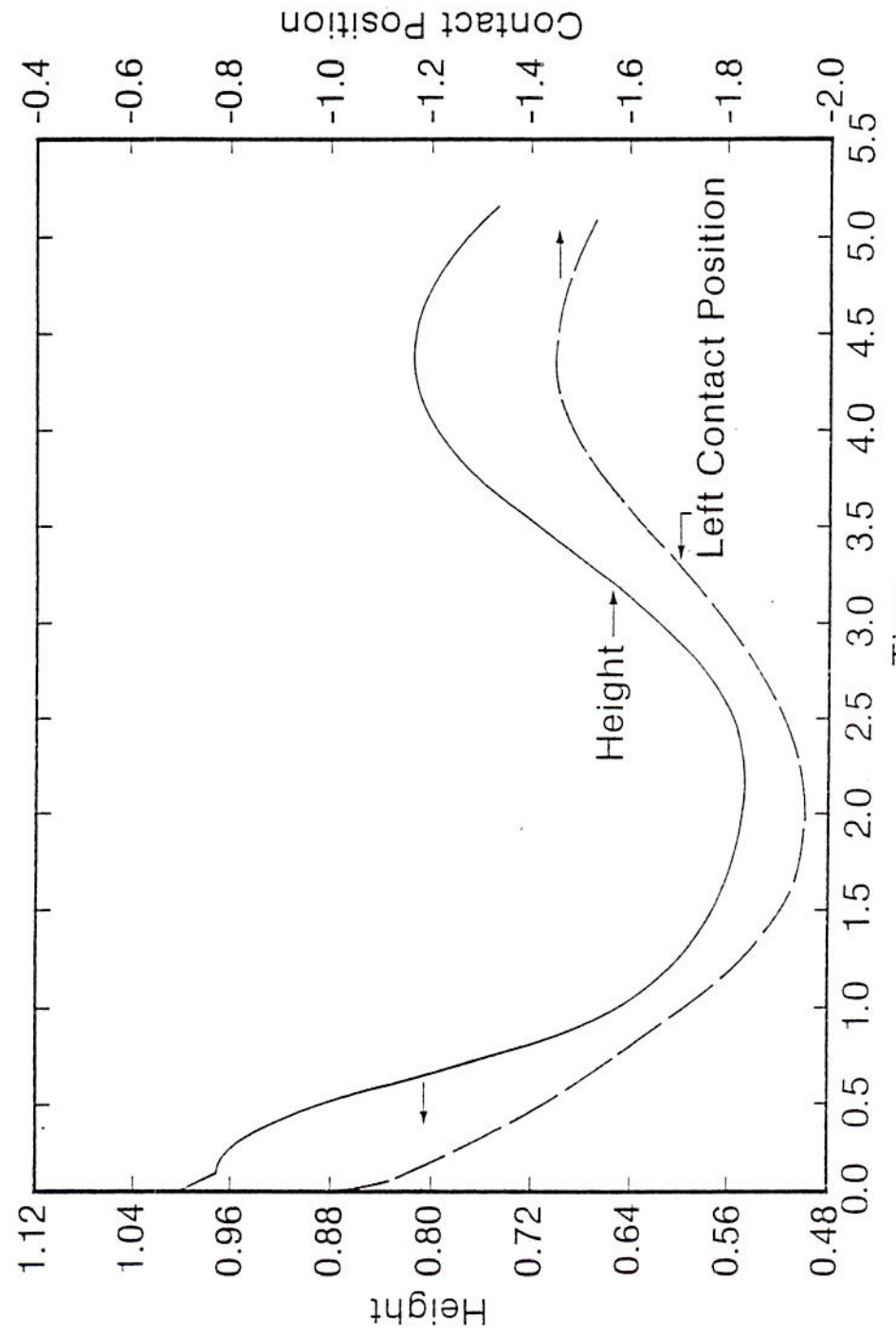

Figure 3. Time variation of crest and left contact position of sequence of Figures 2a, 2b and 2c.

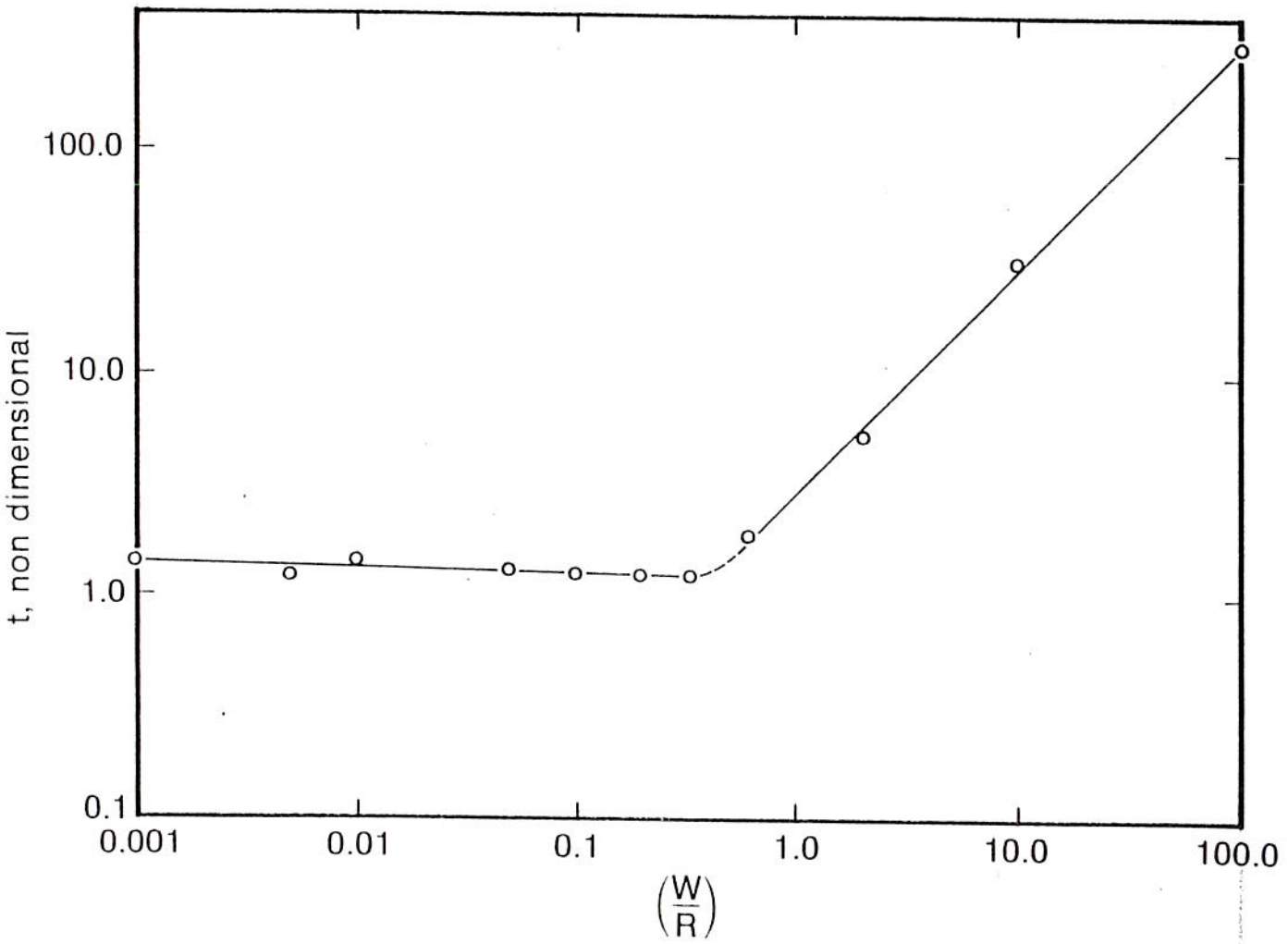

Figure 4. Computed spread times for $\gamma_1=\gamma_2=45°$, based on first arrival to equilibrium half length $\ell=1.65$.

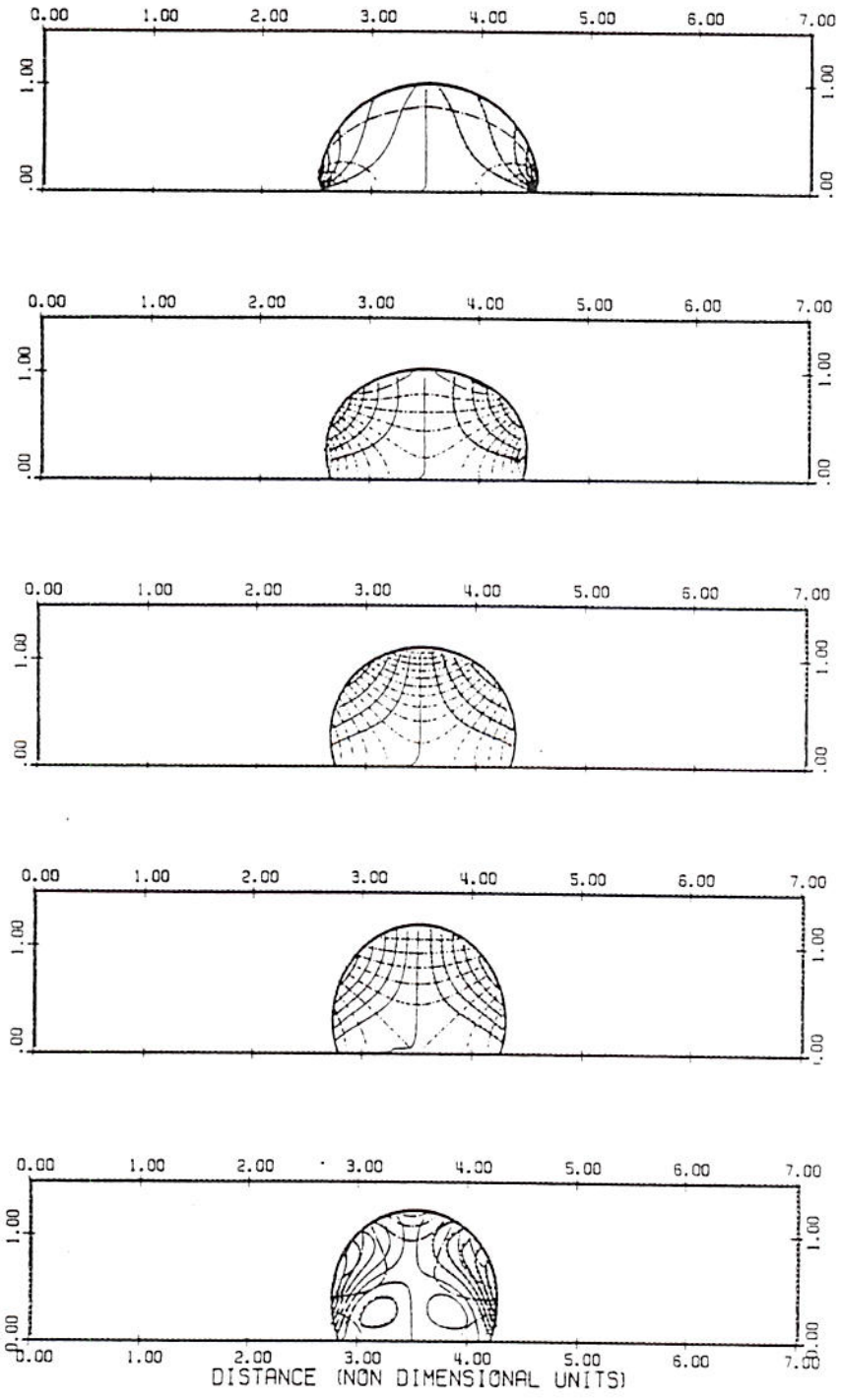

Figure 5a. Time sequence of solutions for $W/R=0.05$, $\gamma_1=\gamma_2=110°$ and $B=0$. See Table II.

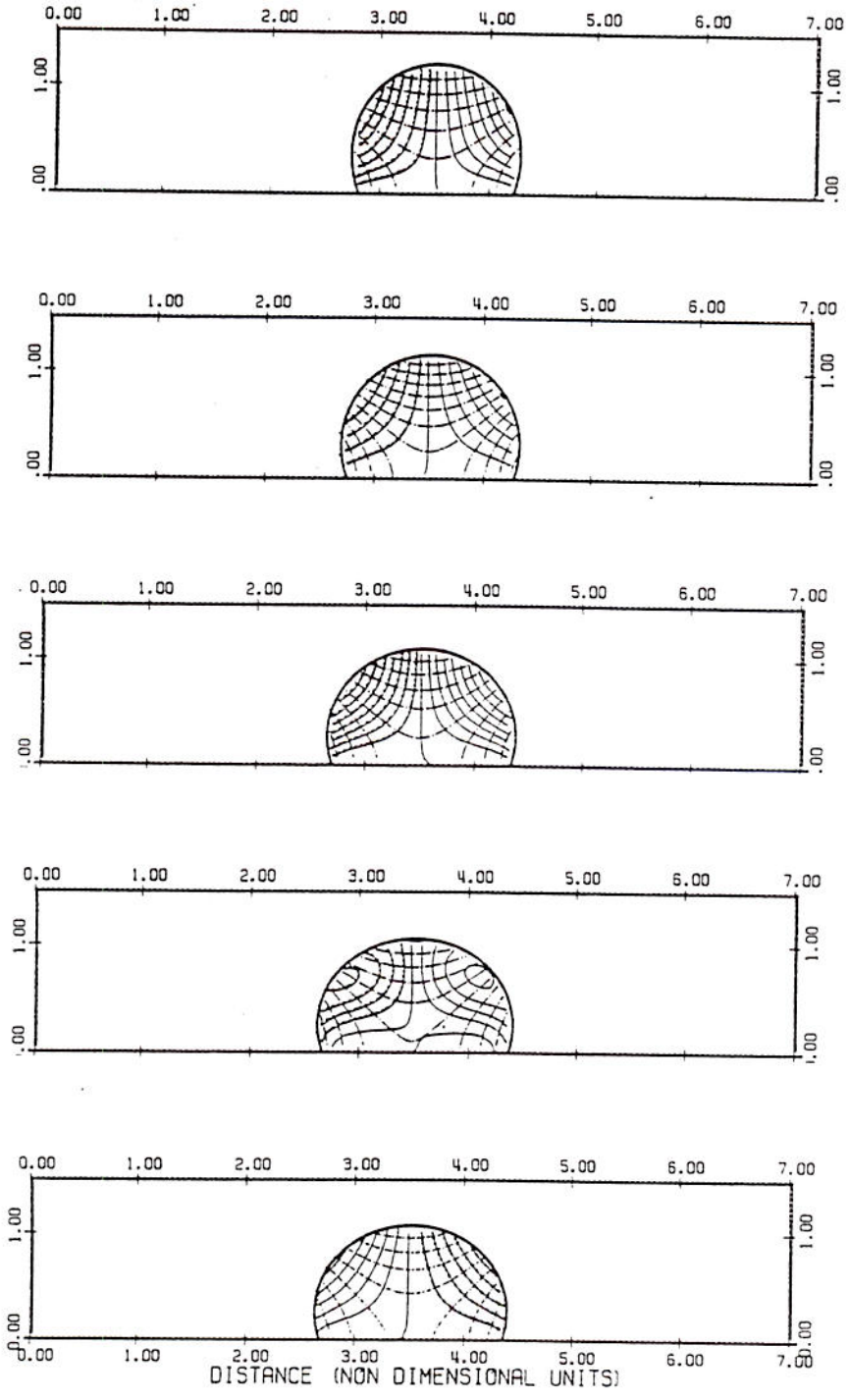

Figure 5b. Continuation of Figure 5a. See Table II.

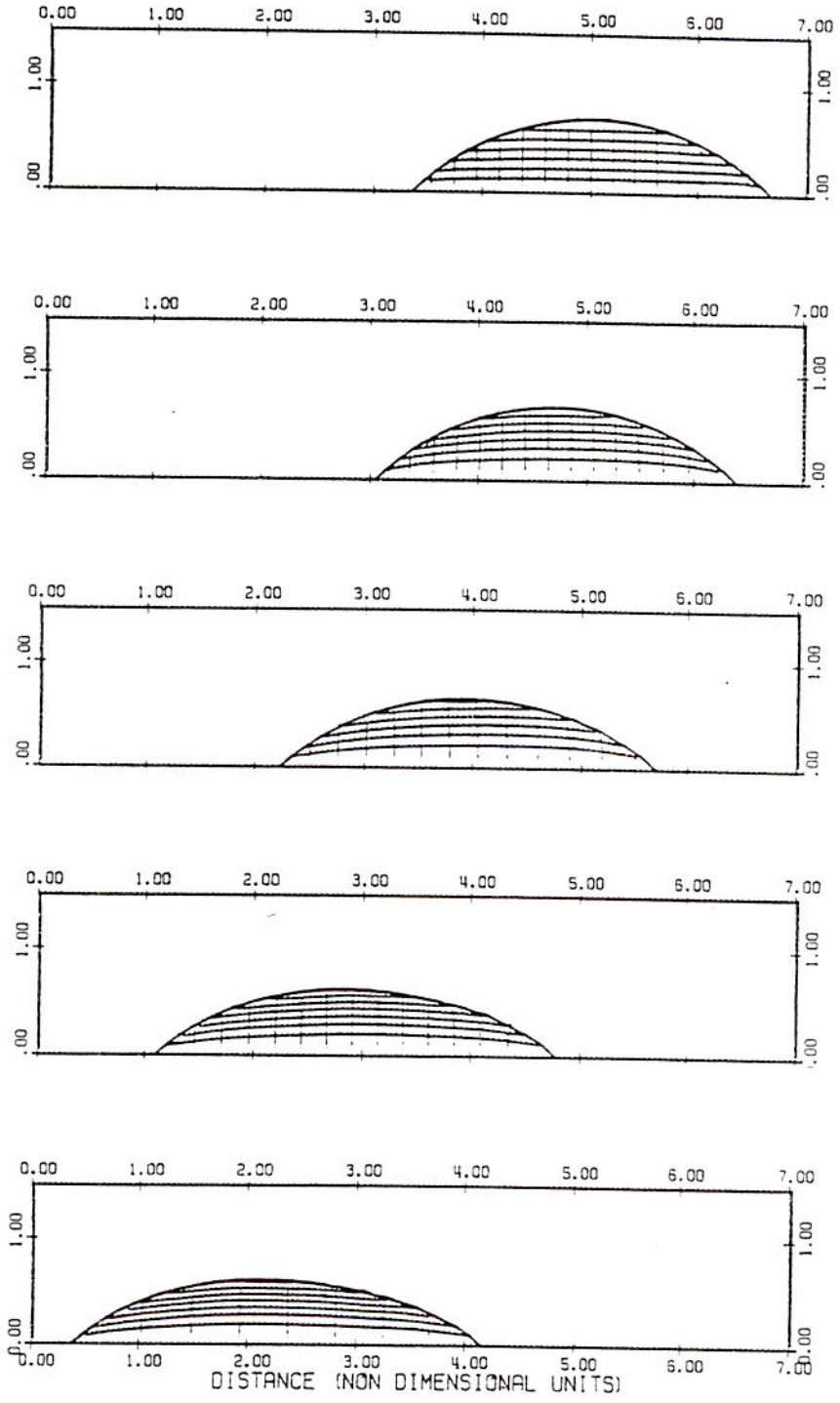

Figure 6. Time sequence of solutions for W/R=0.05, $\gamma_1=\gamma_2=45°$ and B=−0.2. See Table III.